

Building the Pamirs: The view from the underside

Mihai N. Ducea*

Department of Geosciences, University of Arizona, Tucson, Arizona 85721, USA

Valery Lutkov

Vladislav T. Minaev

Geological Institute of the Tajik Academy of Science, 734063, Dushanbe, Tajikistan

Bradley Hacker

Department of Geological Sciences, University of California, Santa Barbara, California 93106-9630, USA

Lothar Ratschbacher

Institut für Geowissenschaften, Technische Universität Bergakademie Freiberg, 09599 Freiberg, Germany

Peter Luffi

Department of Geology and Geophysics, University of Bucharest, Bucharest, 70139, Romania

Martina Schwab

Institut für Geowissenschaften, Universität Tübingen, 72076 Tübingen, Germany

George E. Gehrels

Department of Geosciences, University of Arizona, Tucson, Arizona 85721, USA

Michael McWilliams

Department of Geological and Environmental Sciences, Stanford University, Stanford, California 94305-2115, USA

Jeffrey Vervoort

Department of Geology, Washington State University, Pullman, Washington 99164, USA

James Metcalf

Department of Geological and Environmental Sciences, Stanford University, Stanford, California 94305-2115, USA

*E-mail: ducea@geo.arizona.edu.

¹GSA Data Repository item 2003##, Zircon U-Pb geochronology data, is available online at www.geosociety.org/pubs/ft2003.htm, or on request from editing@geosociety.org or Documents Secretary, GSA, P.O. Box 9140, Boulder, CO 80301-9140, USA.

35

36 **ABSTRACT**

37

38 The Pamir Mountains are an outstanding example of extreme crustal shortening
39 during continental collision that may have been accommodated by formation of a thick
40 crust—much thicker than is currently thought—and/or by continental subduction. We
41 present new petrologic data and radiometric ages from xenoliths in Miocene volcanic
42 rocks in the southeastern Pamir Mountains that suggest that Gondwanan igneous and
43 sedimentary assemblages were underthrust northward, buried to >50–80 km during the
44 early stage of the India-Asia collision, and then heated and partly melted during
45 subsequent thermal relaxation before finally being blasted to the surface. These xenoliths,
46 the deepest crustal samples recovered from under any active collisional belt, provide
47 direct evidence for (1) early Cenozoic thickening of the Pamirs and (2) lower-crustal
48 melting during collision; the xenoliths also suggest that (3) the present mountain range
49 was a steady-state elevated plateau for most of the Cenozoic.

50

51 Keywords: Pamir region, continental collision, subduction, partial melting,
52 orogenic plateaus

53

54 **INTRODUCTION**

55

56 Although many hypotheses have been advanced to explain (1) extreme shortening
57 (e.g. Burtman and Molnar, 1993), (2) melting (e.g. Maheo et al., 2002), (3) continental
58 subduction (e.g. Roecker, 1982; Searle et al., 2001) and (4) the development of high-
59 elevation plateaus in collisional belts—specifically in the Cenozoic Himalayan-Tibetan
60 orogen (e.g., Avouac and Tapponnier, 1993; Yin and Harrison, 2000; DeCelles et al.,
61 2002)—we have few observations with which to test them. Our understanding of these
62 processes is in part limited by the inability to directly observe the deeper crust and upper
63 mantle beneath collisional orogens. Sedimentary and volcanic rocks can be subducted to
64 ultrahigh-pressure depths and subsequently returned to the surface (Coleman and Wang,
65 1995), but their high-temperature history is obscured by retrograde metamorphism and
66 deformation during exhumation (Kohn and Parkinson, 2002). Xenoliths from the lower
67 crust and upper mantle beneath active collisional mountain ranges represent direct
68 samples of these deeper levels and preserve compositional, thermal, and age information
69 that cannot otherwise be obtained. Unfortunately, lower-crustal xenolith localities are rare
70 in such environments (e.g., Hacker et al., 2000).

71

72 In this study, we present new petrographic, thermobarometric, and
73 geochronologic data on deep-crustal xenoliths in Miocene volcanic rocks from the
74 southern Pamir Mountains of central Asia. These samples unambiguously represent parts
75 of the deepest crust beneath the western segment of the Himalayan-Tibetan collisional
76 belt and provide a lower-crustal view for crustal thickening and melting beneath the
77 Pamirs. Specifically, we show that (1) crustal thickening took place in the early stages of
78 the India-Asia collision, (2) the region was a low-relief plateau for most of the Cenozoic,
and (3) the crust partly melted after thermal relaxation.

79

80 **SOUTH PAMIR XENOLITHS**

81

82 Two extension-related Miocene eruptive centers, part of a spectacular belt of
83 Cenozoic magmatism and metamorphism in the southeastern Pamir Mountains,
84 Tajikistan (Fig. 1), contain deep-crustal and mantle xenoliths (Budanova, 1991). The
85 xenolith-bearing volcanic suite is ultrapotassic, ranging from alkali basalt to trachyte and
86 syenite. We analyzed samples of the Dunkeldik pipe belt (Fig. 1B), which is probably a
87 result of local crustal extension (Dmitriev, 1976). Four xenolith types were recognized
88 within a biotite-rich trachyte: felsic eclogites, felsic granulites, mafic eclogites, and
89 phlogopite-garnet websterites (Lutkov, 2003). The websterites are basaltic, contain
90 orthopyroxene, clinopyroxene, garnet, phlogopite, pyrrhotite, and apatite, and may be of
91 mantle origin. The other rocks are unambiguously crustal; their mineral assemblages
92 indicate ultrahigh temperatures and near-ultrahigh pressures. The eclogites consist of
93 omphacite, garnet, and trace rutile, apatite, amphibole, plagioclase, and biotite, whereas
94 the felsic eclogites include these phases plus sanidine, kyanite, quartz, and minor relict
95 plagioclase. The granulites contain garnet, kyanite, quartz, and alkali feldspar and minor
96 graphite and rutile. All but the websterites contain trace zircon and monazite. We
97 determined xenolith eruption ages by $^{40}\text{Ar}/^{39}\text{Ar}$ dating, equilibration pressures and
98 temperatures by using THERMOCALC (Powell and Holland, 1988), and provenance and
99 orogenic history information from zircon and monazite U-Pb ages ($^{40}\text{Ar}/^{39}\text{Ar}$ chronology,
100 thermobarometry, and U-Pb geochronology data tables are available¹).

101 The eruption age of the xenoliths is well constrained by biotite, K-feldspar, and
102 groundmass $^{40}\text{Ar}/^{39}\text{Ar}$ ages (Table DR1) of $10.8\text{--}11.1 \pm 0.15$ Ma from the host trachyte
103 and by biotite ages of 11.2 and 11.5 ± 0.2 Ma from two felsic eclogites (P337, P2104).
104 Optical microscopy and electron-microprobe analysis reveal that the major phases in the
105 xenoliths are well equilibrated—coarse and homogeneous or weakly zoned—and lack
106 retrograde minerals signaling slow cooling or decompression. The garnet websterites
107 were derived from the greatest depths, recording equilibration pressures of $\sim 3\text{--}4$ GPa
108 (Budanova, 1991). Three felsic eclogites and one mafic eclogite equilibrated at
109 temperatures of $1050\text{--}1200$ °C and near ultrahigh pressures of $2.4\text{--}2.7$ GPa (Table DR2).
110 Rare relict hydrous phases and silicate glass as inclusions in the eclogite garnets suggest
111 that dehydration melting accompanied prograde metamorphism. Bulk chemistry of these
112 rocks and their unusual mineralogy (e.g. sanidine-bearing eclogites) also suggest that
113 these rocks have experienced one or two stages of dehydration melting (muscovite and/or
114 biotite) as they were being heated (Patino-Douce and McCarthy, 1998). To our
115 knowledge, these xenoliths are the deepest crustal samples recovered from under any
116 active collisional orogenic belt worldwide.

117

118 **U-Pb GEOCHRONOLOGY**

119

120 Zircons and monazites (Fig. 2) from felsic granulite P1503a and sanidine eclogite
121 P1039 were analyzed in situ by using a 193 nm laser coupled to a Micromass Isoprobe
122 multicollector ICP-MS (inductively coupled plasma–mass spectrometer) (Kidder et al.,
123 2003) (Table DR3). The P1503a zircons are mostly inclusions in garnet and have

124 anhedral, rounded shapes. Crystal shape and the presence of populations of different ages
125 (see subsequent discussion) within a metasedimentary rock strongly suggest that these are
126 detrital zircons. In contrast, the monazites are commonly subhedral matrix minerals
127 grown during prograde metamorphism. During laser ablation, some spots yielded
128 complex isotopic evolution, reflecting age zonation. We report only results that define a
129 single age within 10% error.

130 The calculated bulk composition and mineral-inclusion suite for P1503a suggests
131 that its protolith was a sedimentary, probably two-mica pelite. Equilibration took place
132 above 950 °C and 1.4 GPa, above biotite and phengite dehydration solidi (Castro et al.,
133 2000). The zircon age distribution in P1503a includes distinct peaks at 84–57 Ma, 170–
134 146 Ma, 465–412 Ma, 890 Ma, and 1400 Ma. The youngest zircon ages are 56.7 ± 5.4
135 Ma. Hence, the pelite was either deposited after ~57 Ma or underwent high-grade zircon
136 growth at 57–84 Ma. The lack of 57–84 Ma rims on older zircon grains in the same
137 sample suggest that the hypothesis of a young, post-57 Ma age is more likely. Monazites
138 from P1503a yield U-Pb ages between 34.0 ± 0.5 and 50.3 ± 2.6 Ma.

139 Felsic eclogite P1309 was derived, on the basis of modal calculations, from a
140 calc-alkaline quartz monzonite. It contains zircons whose ages average ca. 75 Ma. Two
141 grains that do not show inheritance or late Cenozoic rim resetting or growth yielded
142 $^{206}\text{Pb}/^{238}\text{U}$ ages of 87.6 ± 6.4 Ma and 63.8 ± 1.5 Ma. Older zircons have $^{206}\text{Pb}/^{238}\text{U}$ ages
143 of ca. 250 Ma, ca. 195 Ma, and ca. 132 Ma. No pre-latest Permian zircons were found in
144 this rock.

145

146 INTERPRETATIONS

147

148 The broad range of detrital-zircon and monazite ages provides a rich data set with
149 which to interpret the tectonic history of the southern Pamir lower crust by reference to
150 the evolution of the Himalayan-Tibetan collision zone. Proterozoic and early Paleozoic
151 ages are similar in the Qiangtang block, the Lhasa block, the Tethyan Himalaya, and the
152 Greater Himalaya, all rifted fragments of Gondwana (Fig. 3; DeCelles et al., 2000; Kapp
153 et al., 2003), suggesting that P1503a was derived from Gondwana crust (Dewey et al.,
154 1988; Yin and Harrison, 2000). The Mesozoic ages preclude derivation of the xenoliths
155 from Indian crust (Hodges, 2000). The 196–132 Ma ages are equivalent to those of the
156 Hindu Kush–Karakoram–southern Pamir active margin arc, which developed through
157 Early Jurassic–Late Cretaceous oceanic subduction and the accretion of the Karakoram,
158 Kohistan, Hindu-Kush, and southern Pamir blocks (Fraser et al., 2001). The predominant
159 ca. 75 Ma zircons, together with the mineral assemblage and calc-alkaline composition,
160 suggest that P1309 was a hydrous (biotite- and/or amphibole-bearing) quartz monzonite
161 emplaced in the upper crust during the Late Cretaceous. We interpret this sample as a
162 fragment of the Kohistan-Ladakh arc thrust sheet emplaced beneath the southern Pamir
163 during the early stage of the Indo-Asian collision (Hodges, 2000). Kohistan-Ladakh arc
164 accretion caused high-grade metamorphism in the Hindu Kush–Karakoram blocks at 80–
165 50 Ma (Fraser et al., 2001) and is likely reflected in the zircon ages from P1503a. High-
166 grade metamorphism and magmatism in the Karakoram began as early as ca. 63 Ma and
167 continues today (Fraser et al., 2001). Most of the P1503a monazite ages as well as zircon
168 rim ages of 20–15 Ma likely reflect this prolonged regional heating.

169 Our results suggest that sedimentary rocks and Jurassic–Late Cretaceous Tethyan-
170 margin igneous rocks of Gondwana affinity were subducted beneath the Pamirs during
171 the early stages of the India-Asia collision. After burial in the early Cenozoic, these
172 supra-crustal rocks were heated, dehydrated, and partly melted from ~35 to ca. 11 Ma.
173 The absence of retrograde metamorphic effects indicates that initial Cenozoic crustal
174 thickening was not succeeded by significant cooling and/or exhumation. A one-
175 dimensional conductive thermal model simulating crustal doubling with initial and
176 boundary conditions appropriate for the Pamir shows that a hypothetical intermediate-
177 composition calc-alkaline rock at 70 km depth should reach >1100 °C after ~30 m.y.,
178 assuming negligible denudation (<0.01 mm/yr). This simple model includes crustal
179 thickening at ca. 50 Ma, followed by thermal relaxation with virtually no denudation, and
180 provides an excellent match to the xenolith geochronology and thermobarometry. Any
181 model that explains the long-term heating and lack of retrogression, must involve
182 minimal exhumation and thus very low erosion rates. The mantle heat flow is assumed to
183 have remained constant throughout thickening.
184

185 **IMPLICATIONS FOR THE INDO-ASIAN COLLISION**

186
187 The potassic, hot, dry, and deep granulitic and eclogitic xenoliths are very
188 unusual, but are similar to xenoliths 1200 km to the east in central Tibet (Hacker et al.,
189 2000). The presence of felsic calc-alkaline, sanidine-bearing eclogites is particularly
190 intriguing (Lutkov, 2003). We propose that a significant component of the thickened
191 crust of the southern Pamir Mountains is an underthrust Late Cretaceous arc—perhaps
192 part of the Ladakh arc as Kapp et al. (2003) and McMurphy et al. (1997) have
193 suggested—on the basis of surface geology and analogies with Tibet. Similarly,
194 subduction of a Cretaceous arc occurred beneath southern Tibet during the development
195 of the Gangdese thrust system (Yin et al., 1994; Yin et al., 1999) The southern Tibetan
196 plateau also contains a large amount of lower crust with P-wave velocities and Poisson’s
197 ratios typical of intermediate-composition calc-alkaline rocks (Owens and Zandt, 1997),
198 similar to what we infer here from the xenoliths. A partly subducted arc may also make
199 up much of the southern Tibetan lower crust.

200 The enigmatic potassic magmatism that characterizes Cenozoic Tibet and the
201 southern Pamirs may have resulted from successive dehydration and melting events that
202 consumed mica and amphibole during thermal reequilibration. Although Turner et al.
203 (1996) argued for a subcontinental lithospheric-mantle origin for the late Cenozoic
204 shoshonitic magmatism in southern Tibet, many of the syenites and trachytes in Tibet and
205 the southern Pamirs could represent partial melts of lower-crustal materials (Meyer et al.,
206 1998; Roger et al., 2000). The xenolith data show that dehydration melting of
207 metasedimentary rocks and calc-alkaline arc-like assemblages took place beneath the
208 southern Pamirs, providing support for a lower-crustal origin of at least some of the high-
209 K magmas in the region. The simplest interpretation is that crustal melting is a result of
210 thermal relaxation. Alternatively, lower crustal melting could have been caused by slab
211 break off and associated mantle upwelling (Maheo et al., 2002).

212 Monazite ages as old as ca. 50 Ma and the absence of retrograde reactions in these
213 lower-crustal xenoliths indicate protracted Cenozoic high-grade metamorphism and
214 minimal exhumation at least through 11 Ma. Despite the large shortening constrained by

215 surface geology (Burtman and Molnar, 1993; Coutand et al., 2002), the lack of
 216 decompression and, by inference, the insignificant surface denudation suggest that the
 217 area that is now the Pamirs formed a low-relief plateau throughout much of the Cenozoic.

218

219 Acknowledgements. Journal reviews by An Yin and Mike Searle significantly improved
 220 the quality of the manuscript.

221

222 REFERENCES CITED

223

224 Avouac, J.P., and Tapponnier, P., 1993, Kinematic model of active deformation in central
 225 Asia: *Geophysical Research Letter*, v. 20, p. 895-898.

226 Budanova, K.T., 1991, *Metamorficheskie porody Tadzhikistana [Metamorphic
 227 formations of Tajikistan]: Akademiya Nauk Tadzhikskoy SSR, Dushanbe, 336 p.
 228 (in Russian).*

229 Burov, E.B., Kogan, M.G., Lyon-Caen, H., and Molnar, P., 1990, Gravity anomalies, the
 230 deep structure, and dynamic processes beneath the Tien-Shan: *Earth and
 231 Planetary Science Letters*, v. 96, p. 367–383.

232 Burtman, V.S., and Molnar, P., 1993, Geological and geophysical evidence for deep
 233 subduction of continental crust beneath the Pamir: *Geological Society of America
 234 Special Paper 281, 76 p.*

235 Castro, A., Corretge, G., El-Biad, M., El-Hmidi, H., Fernandez, C., and Patino-Douce,
 236 A.E., 2000, Experimental constraints on Hercynian anatexis in the Iberian massif,
 237 Spain: *Journal of Petrology*, v. 41, p. 1471–1488.

238 Coleman, R.G., and Wang, X., 1995, *Ultrahigh pressure metamorphism: New York,
 239 Cambridge University Press, 528 p.*

240 Coutand, I., Strecker, M.R., Arrowsmith, J.R., Hilley G, Thiede RC, Korjenkov A,
 241 Omuraliev M, 2002, Late Cenozoic tectonic development of the intramontane
 242 Alai valley (Pamir-Tien Shan region, central Asia); An example of
 243 intracontinental deformation due to the Indo-Eurasia collision, 2002, *Tectonics*, v.
 244 21, art no. 1053.

245 DeCelles, P.G., Gehrels, G.E., Quade, J., LaReau, B., and Spurlin, M., 2000, Tectonic
 246 implications of U-Pb zircon ages of the Himalayan orogenic belt in Nepal:
 247 *Science*, v. 288, p. 497–499.

248 DeCelles, P.G., Robinson, D.M., and Zandt, G., 2002, Implications of shortening in the
 249 Himalayan fold-thrust belt for uplift of the Tibetan plateau: *Tectonics*, v. 21,
 250 p. 10.1029/2001TC001322.

251 Dewey, J.F., Shackleton, R.M., Chengfa, C., and Yiyin, S., 1988, The tectonic evolution
 252 of the Tibetan plateau: *Royal Society of London Philosophical Transactions*, ser.
 253 A, v. 327, p. 397–413.

254 Dmitriev, E.A., 1976, *Kainozoiskie kalievye schelochnye porody Vostochnogo Pamira
 255 [Cenozoic potassium-rocks of Eastern Pamir]: Dushanbe, Akademiya Nauk
 256 Tadzhikskoy SSR, 171 p. (in Russian).*

257 Fraser, J.E., Searle, M.P., Parrish, R.R., and Noble, S.R., 2001, Chronology of
 258 deformation, metamorphism, and magmatism in the southern Karakoram
 259 Mountains: *Geological Society of America Bulletin*, v. 113, p. 1443–1455.

- 260 Gansecki, C.A., Mahood, G.A., and McWilliams, M.O., 1996, Ar/Ar geochronology of
261 rhyolites erupted following collapse of the Yellowstone caldera, Yellowstone
262 Plateau volcanic field: Implications for crustal contamination: *Earth and Planetary
263 Science Letters*, v. 142, p. 91–107.
- 264 Hacker, B.R., Gnos, E., Ratschbacher, L., Grove, M., McWilliams, M., Sobolev, S.V.,
265 Wan, J., and Zhenhan, W., 2000, Hot and dry deep crustal xenoliths from Tibet:
266 *Science*, v. 287, p. 2463–2466.
- 267 Hildebrand, P.R., Noble, S.R., Searle, M.P., Waters, D.J., and Parrish, R.R., 2001, Old
268 origin for an active mountain range: Geology and geochronology of the eastern
269 Hindu Kush, Pakistan: *Geological Society of America Bulletin*, v. 113, p. 625–
270 639.
- 271 Hodges, K.H., 2000, Tectonics of the Himalaya and southern Tibet from two
272 perspectives: *Geological Society of America Bulletin*, v. 112, p. 324–350.
- 273 Kapp, P., Murphy, M.A., Yin, A., Harrison, T.M., Ding, L., Guo, J., 2003, Mesozoic and
274 Cenozoic tectonic evolution of the Shiquanhe area of western Tibet: *Tectonics*,
275 v. 22, 10.1029/TC001332, p. 1–14.
- 276 Kidder, S., Ducea, M.N., Gehrels, G.E., Patchett, P.J., and Vervoort, J., 2003, Tectonic
277 and magmatic development of the Salinian Coast Ridge Belt, California:
278 *Tectonics*, (in press).
- 279 Kohn, M.J., and Parkinson, C.D., 2002, Petrologic case for Eocene slab breakoff during
280 the Indo-Asian collision: *Geology*, v. 30, p. 591–594.
- 281 Lutkov, V.S., 2003, Petrochemical evolution and genesis of potassium pyroxenite-
282 eclogite granulite association in the mantle and crustal xenoliths from Neogene
283 fergusonites of South Pamir, Tajikistan, v. 3, p. 254–265.
- 284 Maheo, G., Guillot, S., Blichert-Toft, J., Rolland, Y., and Pecher, A., 2002, A slab
285 breakoff model for the Neogene thermal evolution of the south Karakorum and
286 south Tibet: *Earth and Planetary Science Letters*, v. 195, p. 45–58.
- 287 McMurphy, M.A., Yin, A., Harrison, T.M., Durr, S.B., Chen, Z. et al., 1997, Significant
288 crustal shortening in south-central Tibet prior to the Indo-Asian collision,
289 *Geology*, v. 25, p. 719–722.
- 290 Meyer, B., Tapponnier, P., Bourjot, L., Metivier, F., Gaudemer, Y., Peltzer, G., Guo, S.,
291 and Chen, Z., 1998, Crustal thickening in Gansu-Qinghai, lithospheric mantle
292 subduction, and oblique, strike-slip controlled growth of the Tibet plateau:
293 *Geophysical Journal International*, v. 135, p. 1–47.
- 294 Owens, T.J., and Zandt, G., 1997, Implications of crustal property variations for models
295 of Tibetan plateau evolution: *Nature*, v. 387, p. 37–43.
- 296 Patino-Douce, A.E., and McCarthy, T.C., 1998, Melting of crustal rocks during
297 continental collision and subduction, *in* Hacker, B.R., and Liou, J.G., ed., *When
298 continents collide*: Dordrecht, Netherlands, Kluwer Academic, p. 27–55.
- 299 Pavlis, G.L., and Das, S., 2000, The Pamir Hindu-Kush seismic zone as a strain marker
300 for flow in the upper mantle: *Tectonics*, v. 19, p. 103–115.
- 301 Powell, R., and Holland, T.J.B., 1988, An internally consistent data set with uncertainties
302 and correlations: 3. Applications to geobarometry, worked examples and a
303 computer program: *Journal of Metamorphic Geology*, v. 6, p. 173–204.
- 304 Roecker, S.W., 1982, Velocity structure of the Pamir–Hindu Kush region: Possible
305 evidence for subducted crust: *Journal of Geophysical Research*, v. 87, p. 945–959.

- 306 Roger, F., Tapponnier, P., Arnaud, N., Scharer, U., Brunel, M., Xu, Z.Q., and Yang, J.S.,
 307 2000, An Eocene magmatic belt across central Tibet: Mantle subduction triggered
 308 by the Indian collision? *Terra Nova*, v. 12, p. 102-108.
- 309 Searle, M., Hacker, B.R., and Bilham, R., 2001, The Hindu Kush seismic zone as a
 310 paradigm for the creation of ultrahigh-pressure diamond- and coesite-bearing
 311 continental rocks: *Journal of Geology*, v. 109, p. 143-153.
- 312 Stacey, J.S., and Kramers, J.D., 1975, Approximation of terrestrial lead isotope evolution
 313 by a two-stage model: *Earth and Planetary Science Letters*, v. 26, p. 207–221.
- 314 Turner, S., Arnaud, N., Liu, J., Rogers, N., Hawkesworth, C., Harris, N., Kelley, S., Van
 315 Calsteren, P., and Deng, W., 1996, Postcollision, shoshonitic volcanism on the
 316 Tibetan plateau: Implications for convective thinning of the lithosphere and the
 317 source of ocean island basalts: *Journal of Petrology*, v. 37, p. 45–71.
- 318 Yin, A., Harrison, T.M., Ryerson, F.J., Chen, W.J., Kidd, W.S.J., and Copeland, P., 1994,
 319 Tertiary structural evolution of the Gangdese thrust system, southeastern Tibet:
 320 *Journal of Geophysical Research*, v. 99, p. 18175-18201.
- 321 Yin, A., Harrison, T.M., Murphy, M.A., Grove, M., Nie, S., Ryerson, F.J., Feng, W.X.,
 322 and Le, C.Z., 1999, Tertiary deformation history of southeastern and southwestern
 323 Tibet, during the Indo-Asian collision: *Geological Society of America Bulletin*, v.
 324 111, p. 1644-1664.
- 325 Yin, A., and Harrison, T.M., 2000, Geologic evolution of the Himalayan-Tibetan orogen:
 326 *Annual Review of Earth and Planetary Sciences*, v. 28, p. 211–280.

327

328

329 **FIGURE CAPTIONS**

330

331 Figure 1. A: Central, and southern Pamir Region of Tajikistan and western China with
 332 major sutures and magmatic belts on the basis of U-Pb zircon geochronology. Pre-
 333 Cenozoic terrane division is primarily from Yin and Harrison (2000). B: Location of
 334 Dunkeldik xenolith-bearing volcanic field in southeast Pamirs.

335 Figure 2. Microphotographs of samples analyzed for U-Pb geochronology. A: Zircon
 336 inclusion in garnet from P1309 (plane-polarized light). B: Metamorphic monazite in
 337 metapelite P1503a (plane-polarized light). C: Detrital-zircon inclusions in garnet in
 338 P1503a (cross-polarized light).

339 Figure 3. A: Cumulative-probability plots illustrating age groups of zircons from
 340 southeastern Pamir xenoliths (red; this paper) compared with two southeastern Pamir
 341 monzogranite samples (Schwab, unpublished work) and basement outcrops of Qiangtang
 342 block of central Pamirs (Schwab, unpublished work) and Tibet (Kapp et al., 2003).
 343 Lower part of diagram shows distribution of detrital-zircon ages of Tethyan and Greater
 344 Himalaya successions of southern Tibet and Himalayas (DeCelles et al., 2000).
 345 Proterozoic and Paleozoic xenolith zircon ages are most likely of Qiangtang–Lhasa–
 346 Greater Himalaya, and thus Gondwana, origin. B: Zircon, monazite, and uraninite ages of
 347 magmatic and high-grade sedimentary successions of Hindu Kush–Karakoram
 348 (Hildebrand et al., 2001; Fraser et al., 2001) and Kohistan-Ladakh-Lhasa block (Schwab,
 349 unpublished work) of Pamirs and Tibet.

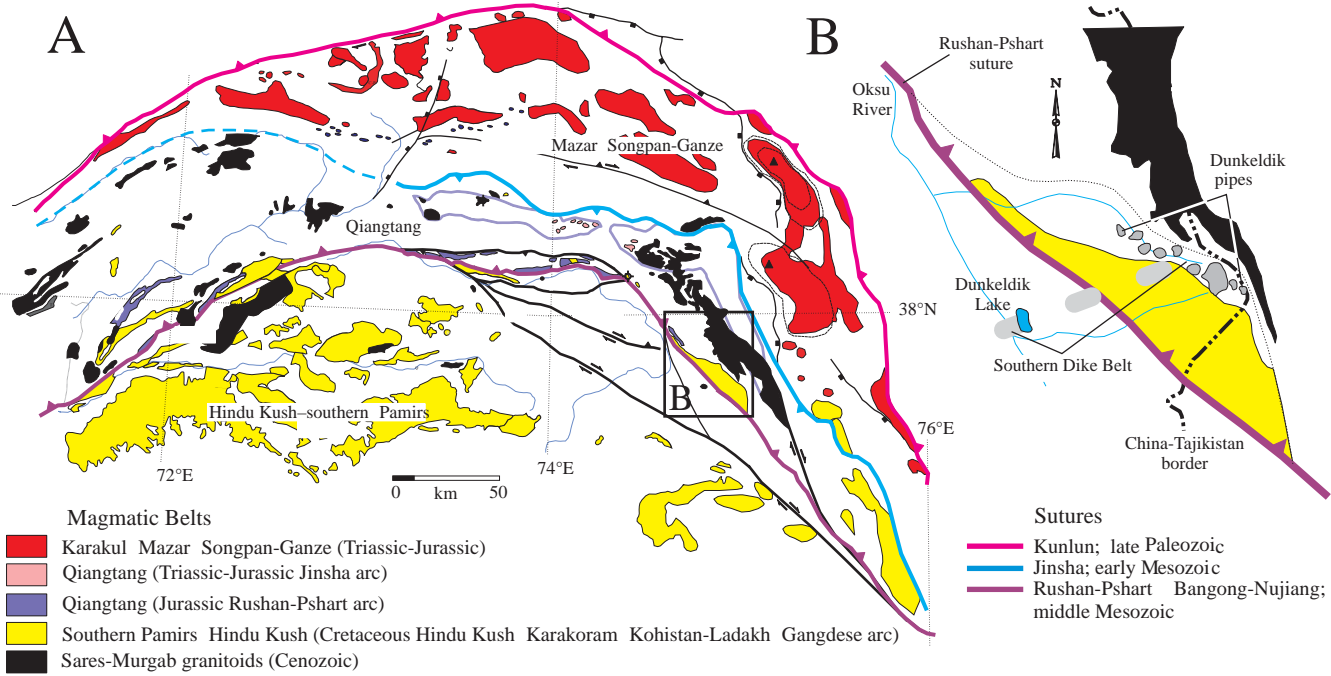


Figure 1, Ducea et al., G19707

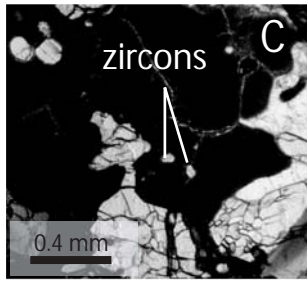
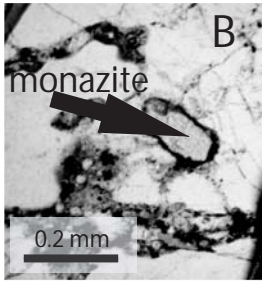
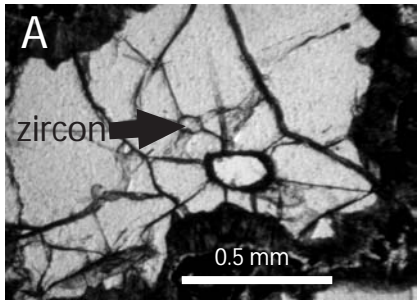


Figure 2, Ducea et al., G19707

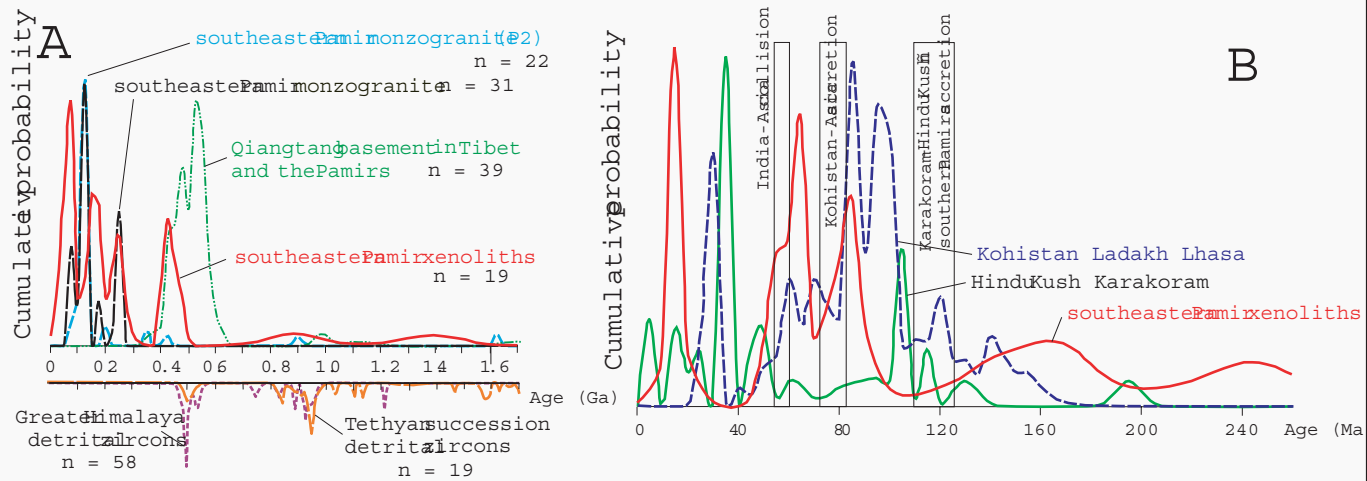


Figure 3, Ducea et al., G19707